

Context and aim

Surges are key ejections in the solar atmosphere due to their close relation to many other phenomena like UV bursts and jets. Even though surges have been observed for decades now, questions regarding their physical properties such as temperature and density, as well as their impact on upper layers of the solar atmosphere remain open. Our purpose is to address the current lack of inverted models and diagnostics of surges, as well as characterizing their fundamental properties.

Methods

We have analyzed IRIS ([de Pontieu et al. 2014](#)) observations of surges ([Figure 1](#)) acquired between 2016-04-13 and 2016-04-14 within active region AR NOAA 12529 at (X,Y)= (0",269"). The data set contains four dense 64-step raster scans whose exposure time is 18 s for the far-UV and 9 s for the near-UV.

We have obtained representative Mg II h&k line profiles in each raster using k -means: a clustering algorithm that classifies a set of n samples in k disjoint clusters ([Pedregosa et al. 2011](#)).

We have performed inversions of these representative profiles using the STIC code ([de la Cruz Rodríguez et al. 2019](#)), which assumes NLTE and includes partial frequency redistribution effects of scattered electrons.

We have studied the transition region counterpart of surges through the O IV 1399.8 Å and 1401.2 Å lines, also performing density diagnostics based on the ratio of these lines.

We have used 2.5D numerical experiments of surges carried out with the Bifrost code ([Gudiksen et al. 2011](#)) for comparisons.

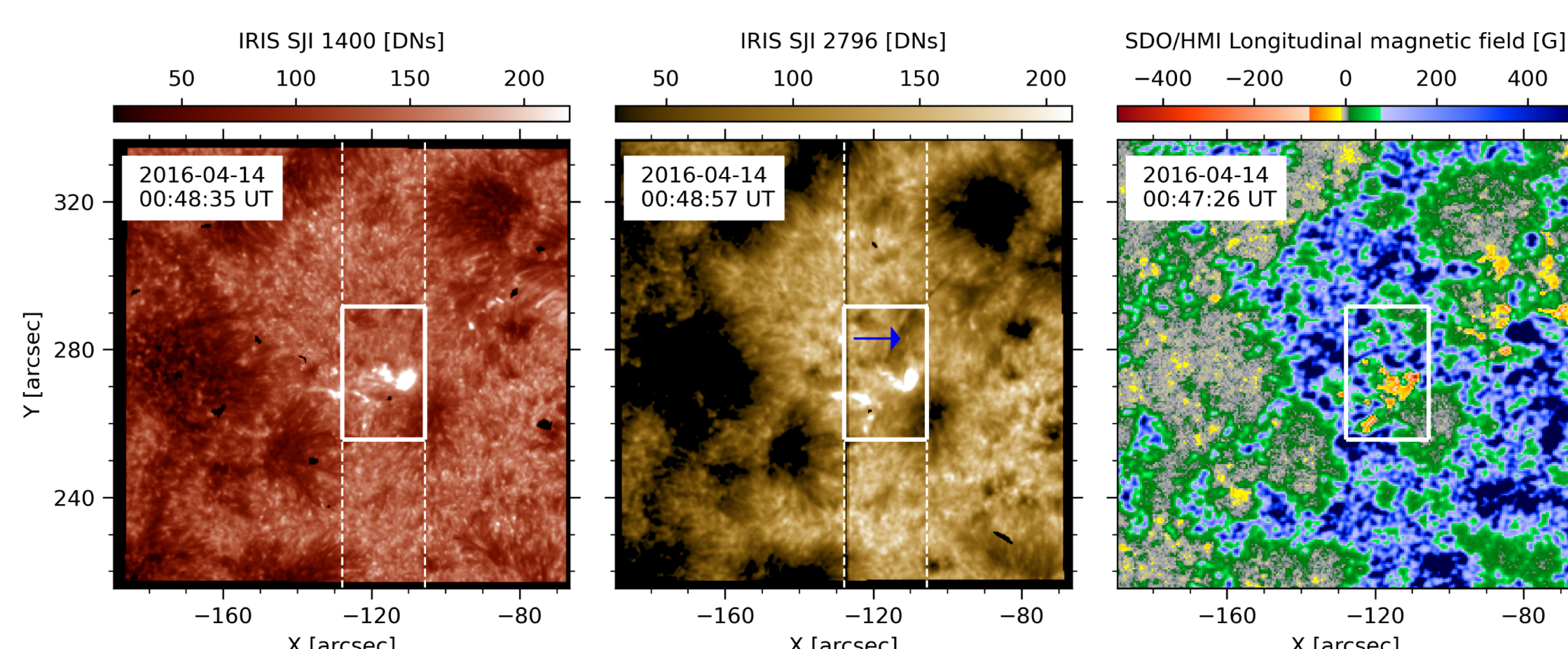


Figure 1. Context image showing IRIS SJI 1400, IRIS SJI 2796, and SDO/HMI line-of-sight magnetogram. The solid box frames the portion of the FoV studied. The blue arrow indicates one of the observed surges that appears next to a UV burst.

In [Figure 2](#), the first column illustrates the surge of Raster 3 delimited by a black contour. For each raster, we use the k -means method to group the Mg II h&k line profiles in 160 clusters. The labels map from the k -means for Raster 3 (second column) show that the surge and UV burst have clear different Mg II h&k profiles from other regions. The other panels contain the results from the inversions for a given optical depth, indicating that the surge is mostly cooler and it has smaller electron number density than their surroundings. In [Figure 3](#), the leftmost column contains the spectral information for two particular locations within the surge, showing that the observed profile (grey), the representative one from k -means (red), and the inverted one (cyan) are very similar: a fact that gives robustness to our results. The rest of the columns illustrate the stratification derived from the inversions with their corresponding uncertainties, thus being able to determine in which optical depths our results are reliable. [Figure 4](#) contains the statistical results obtained in each surge of the four rasters analyzed. The stacked histograms by raster show that the different surges have similar properties (e.g., the most probable temperature is around 6 kK). The stacked histograms by $\log_{10}(\tau)$ illustrate the variation of the physical parameters with the optical depth: cooler plasma with smaller electron number density in the surges is located deeper in the atmosphere.

One of the most striking results is the finding of emission in the O IV 1399.8 Å and 1401.2 Å lines in surges ([Figure 5](#)). The brightest O IV regions are located within the surges and/or in their boundaries following the threads (see arrow in the image). This provides support to the theoretical findings by [Nóbrega-Siverio et al. 2018](#), which showed that surges can show enhanced transition region emission. In addition, it allows us to determine the electron density of the O IV emitting layers, obtaining values between -2.5×10^{10} and 10^{13} cm^{-3} . The results from the simulations ([Figure 6](#)) show similarities with the observations: cooler plasma with smaller electron number density in the surges is located in lower regions of the atmosphere. In addition, we can explain the thread-like structure as well as the location of the O IV regions (red contour at $T = 200 \text{ kK}$) with respect to the core of the surges (green contour at $T = 6 \text{ kK}$) which is detected in the observations (see [Figure 5](#)).

Conclusions

- Combining machine learning techniques and inversions, we obtain that the mid- and low-chromosphere of the surges are characterized by temperatures mainly around $T = 6 \text{ kK}$ at $-6.0 \leq \log_{10}(\tau) \leq -3.2$, with a high degree of reliability. For the electronic number densities, n_e , and line-of-sight velocity, V_{LOS} , the most reliable results from the inversions are from $-6.0 \leq \log_{10}(\tau) \leq -4.8$, with n_e ranging from -1.6×10^{11} to 10^{12} cm^{-3} and V_{LOS} of a few km s^{-1} .
- We find, for the first time, evidence of enhanced O IV 1399.8 Å and 1401.2 Å emission within surges, indicating that these phenomena have a considerable impact in the transition region even in the weakest far-UV lines. The O IV emitting layers of the surges have an electron number density ranging from -2.5×10^{10} to 10^{13} cm^{-3} . We also provide theoretical support in terms of the topology and of the location of the O IV emission within the surges through the simulations.

Results

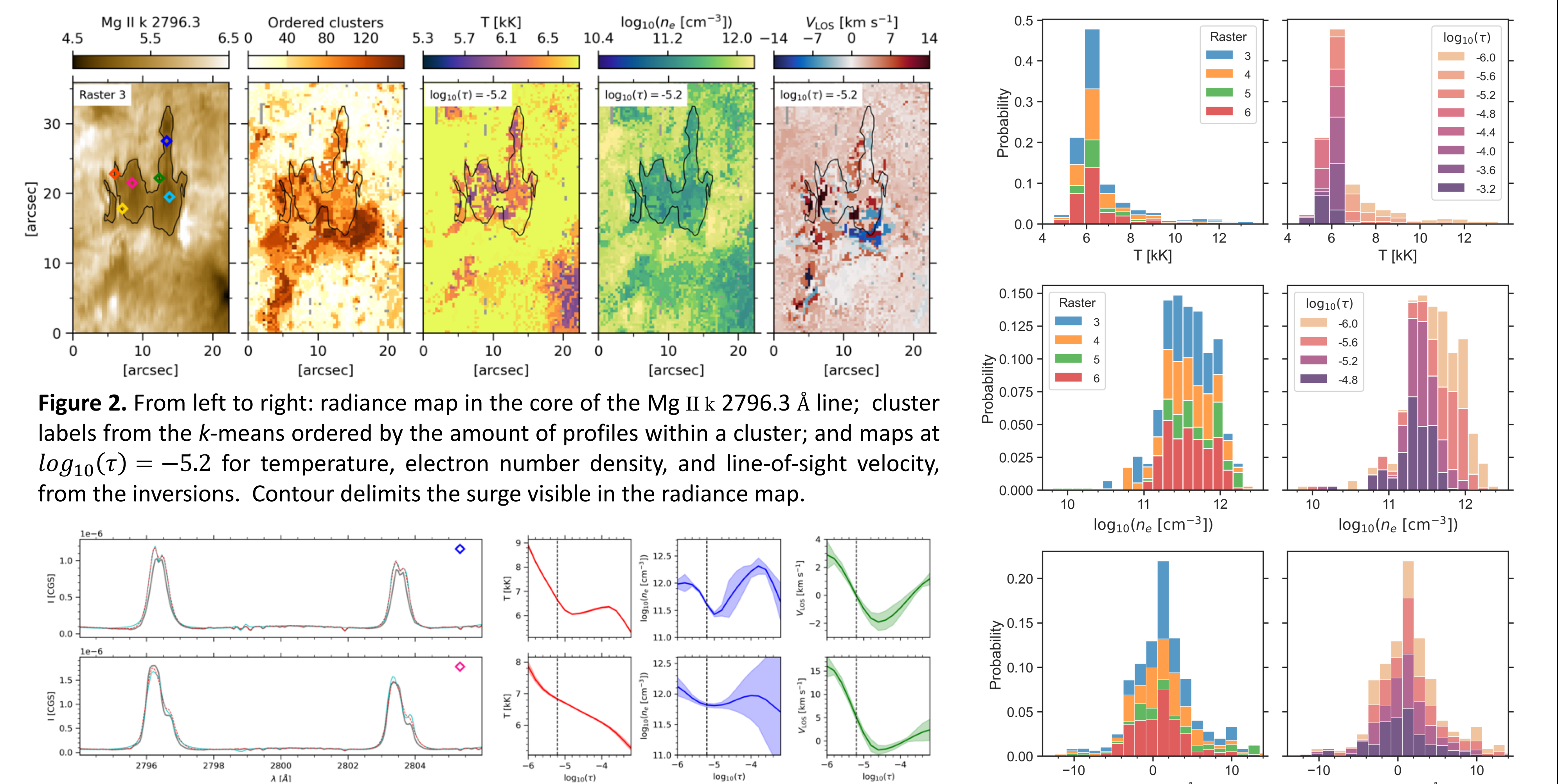


Figure 2. From left to right: radiance map in the core of the Mg II k 2796.3 Å line; cluster labels from the k -means ordered by the amount of profiles within a cluster; and maps of $\log_{10}(\tau) = -5.2$ for temperature, electron number density, and line-of-sight velocity, from the inversions. Contour delimits the surge visible in the radiance map.

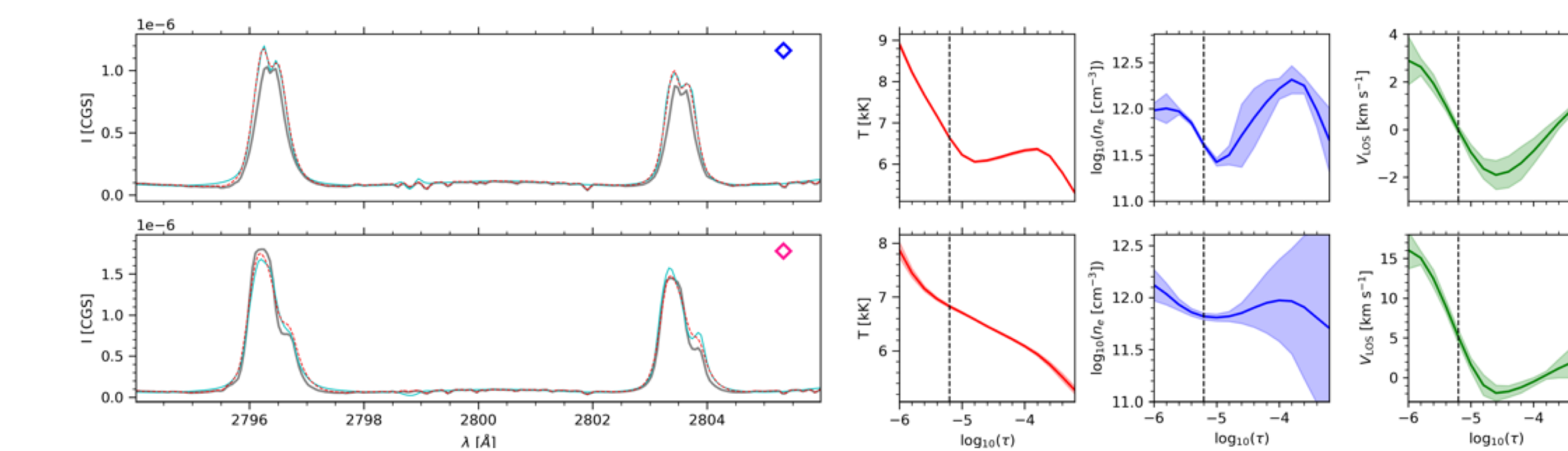


Figure 3. Left: observed Mg II h&k profile (grey), corresponding representative profile obtained with k -means (red), and the inverted profile using the STIC code (cyan) for the blue and pink locations in [Figure 2](#). Right: results from the inversions for T , n_e , and V_{LOS} as functions of $\log_{10}(\tau)$ with their inversion uncertainties ($\pm\sigma$). The vertical line in these plots at $\log_{10}(\tau) = -5.2$ indicates the optical depth shown in [Figure 2](#).

Figure 4. Statistics for T , n_e , and V_{LOS} within the surges for the optical depths in which inversions are more reliable. Columns show stacked histograms organized by raster (left) and by $\log_{10}(\tau)$ (right).

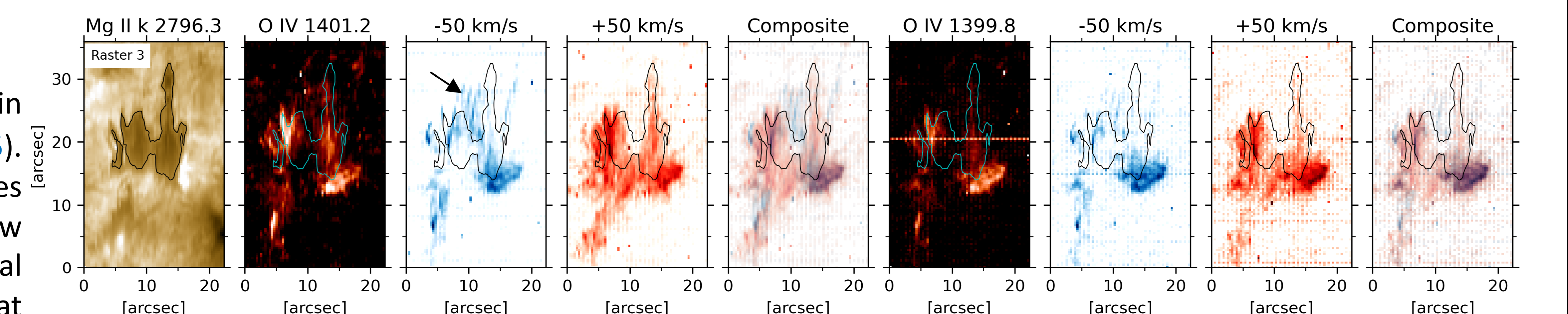


Figure 5. From left to right: radiance maps in the core of the Mg II k 2796.3 Å line (first column); in the core of the O IV 1401.2 Å line (second column); and in its blue and red wings at -50 and 50 km s^{-1} (third and fourth columns, respectively); and composite image of both wings (fifth column). Equivalent maps are plotted for the O IV 1399.8 Å line (sixth-ninth columns).

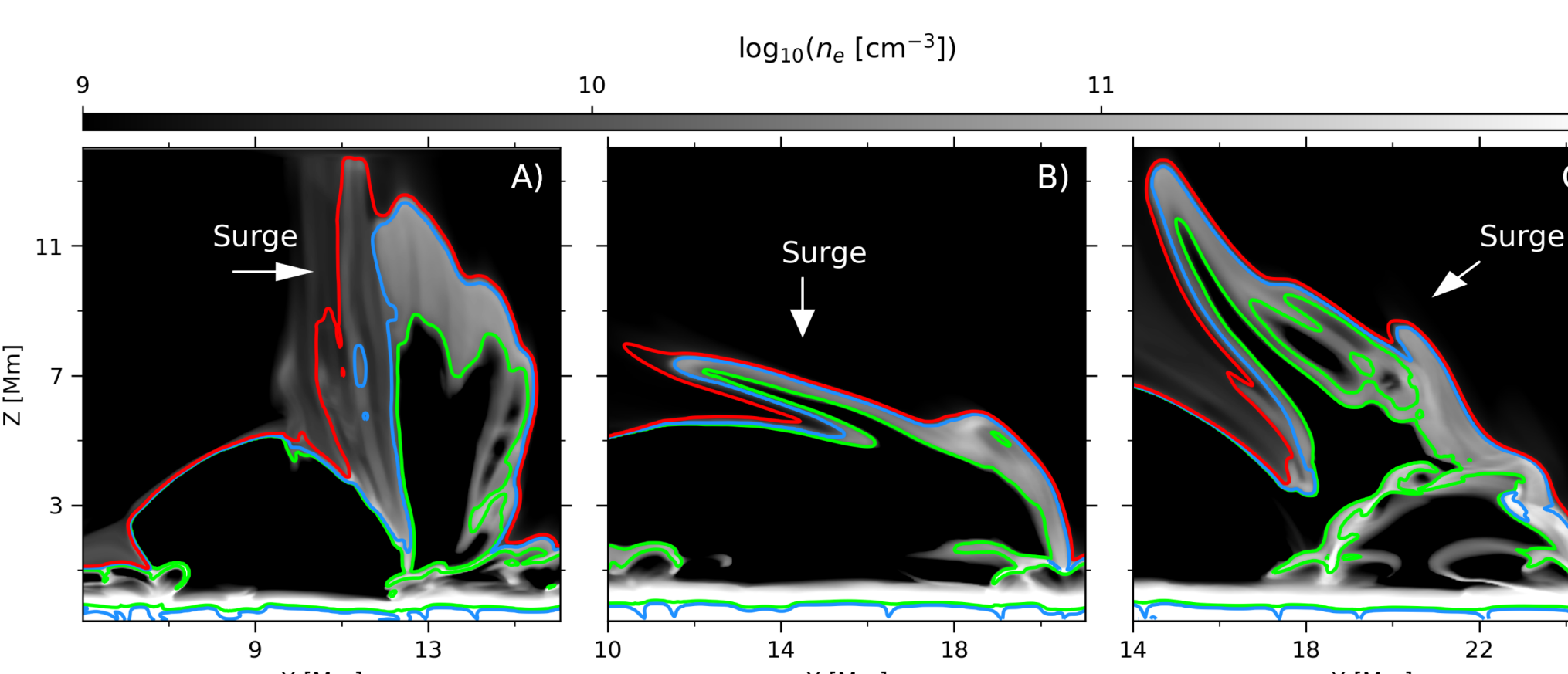


Figure 6. Electron number density for three different simulated surges. Contours of temperature are superimposed for $T = 6 \text{ kK}$ (green), $T = 10 \text{ kK}$ (blue) and $T = 200 \text{ kK}$ (red). Panel A: surge from the [Nóbrega-Siverio et al. 2016](#) numerical experiment. Panels B and C: surges from the simulations by [Nóbrega-Siverio et al. 2017, 2018](#).